Phase structure and molecular dynamics of liquid-crystalline side-on organosiloxane tetrapodes

D. Filip,[1,2] C. Cruz,[1,3] P. J. Sebastião,[1,3] M. Cardoso,[1] A. C. Ribeiro,[1,3] M. Vilfan,[4] T. Meyer,[5] P. H. J. Kouwer,[5] and G. H. Mehl[5]

[1]*Centro de Física da Matéria Condensada, Universidade de Lisboa, Av. Prof. Gama Pinto 2, 1649-003 Lisboa, Portugal*

[2]*"Petru Poni" Institute of Macromolecular Chemistry, Aleea Gr. Ghica Voda 41 A, 700487 Iasi, Romania*

[3]*IST, TU Lisbon, Av. Rovisco Pais, 1049-001 Lisboa, Portugal*

[4]*Jozef Stefan Institute, Jamova 39, SI-1000 Ljubljana, Slovenia*

[5]*Department of Chemistry, University of Hull, Cottingham Road, Hull HU6 7RX, United Kingdom*

(Received 7 April 2009; published 19 January 2010)

X-ray diffraction and proton NMR relaxation measurements were carried out on two liquid-crystalline organosiloxane tetrapodes with side-on mesogenic groups, exhibiting nematic and smectic-*C* phases, and on a monomeric analog. Packing models for the mesophases exhibited by these systems are proposed on the basis of x-ray diffraction data. As a consequence of microsegregation, the aromatic cores are packed in between two sublayers formed by a mixture of interdigitated aliphatic and siloxane chains. The mixed sublayers are characteristic for the tetrapodes with side-on mesogenic groups presented in this work and have not been observed in tetrapodes with terminally attached mesogens. The tilt angle in the smectic-*C* phase is found very large, i.e., $\sim 61^\circ - 62^\circ$. Notably, smectic-*C* clusters are present also in the whole temperature range of the nematic phase. NMR relaxometry yields T_1^{-1} dispersions clearly different from those of conventional calamitics. The influence of molecular tendency to form interdigitated structures is evidenced by frequency-dependent relaxation rate in the isotropic phase—indicating the presence of ordered clusters far above the phase transition—and by the diminished role of molecular self-diffusion in ordered phases. Nematiclike director fluctuations are the dominating relaxation mechanism whereas the translational displacements are strongly hindered by the interdigitation of dendrimer arms.

DOI: 10.1103/PhysRevE.81.011702 PACS number(s): 61.30.−v, 76.60.−k

I. INTRODUCTION

Liquid-crystalline dendrimers are unique materials that combine the hyperbranched monodisperse molecular structure of dendrimers with the spatial self-organizing properties of mesomorphic systems [1]. Dendrimer molecules are obtained through specific stepwise synthesis procedures, which give rise to treelike structures of increasing size depending on the number of synthetic steps performed. This process determines the number of free peripheral branches of the dendrimer, which grows geometrically with the level of branching and defines the dendrimer generation [2]. Using this synthetic strategy, it is possible to build objects with molecular dimensions up to a scale comparable to those of surfactant micelles or vesicular aggregates [3]. Dendrimer properties in solution [4] as well as their rheological [5] and glass transition [6] behavior suggest that open interpenetrated structures characteristic of low-generation materials give way to a more compact spherical shape beginning at generation 3. In this way, a wide variety of different macromolecules can be produced with interesting supramolecular organizations and properties [1,7]. They allow for promising applications of dendrimers as drug [8] and contrast agent carriers [9], gene transfer agents [10], and nanosized carriers in combinatorial synthesis [11].

Within this interesting class of highly functional compounds, liquid-crystalline dendrimers are of special interest because of the possibility of creating controlled supermolecules that are able to self-organize into various mesomorphic phases with multifunctional properties. They could provide, for example, an original concept for molecular electronic-based devices [7]. Liquid-crystalline dendrimers are interesting also from the fundamental point of view as they combine two types of elements with opposite tendencies: the anisotropic mesogenic units, which tend to self-organize into ordered structures, and the isotropic dendritic core with the disordering effect on the packing of molecules. There is a competition between the need of the molecular shape to remain spherical and the ability of the supermolecular system to be deformed in order to fit within the mesomorphic environment. In the case of low-generation dendrimers, the dendritic cores are easily deformed so that they can adapt to the packing of the mesogenic groups [1]. The coexistence of entities with different packing tendencies, i.e., of isotropic cores and anisotropic mesogenic parts, predetermines a microsegregation which leads to the formation of mesophases with closely packed and interconnected mesogenic units [12].

The simplest example of liquid-crystalline dendrimers are those of generation zero, which are also called multipodes. They possess a single level of branching, resulting in a starlike flexible core with a mesogenic unit at the end of each dendrimer arm. The phase structures and physical properties of such materials depend on the degree of flexibility of the dendritic core, on the mutual interacting properties of mesogenic units, and also on the type of linking (e.g., end-on vs side-on) between the dendrimer core and the mesogenic units. On studying multipodes, the effect of the complexity of the inner hyperbranched dendritic core, that appeared as an important aspect in previous nuclear magnetic resonance (NMR) relaxation studies on higher generation dendrimers [13–15], is reduced. Mesophases formed by multipodes exhibit thus an intermediate degree of complexity between that

of low-molecular-weight liquid crystals and that of higher generation dendrimers.

In the present study we are dealing with two organosiloxane tetrapodes of generation zero which exhibit nematic and smectic-*C* (Sm*C*) phases. They have mesogenic units attached in a side-on position in contrast to tetrapodes with end-on mesogenic groups which were the topic of a previous study [16]. The mesogenic units have symmetric chemical structure in one of the tetrapodes and asymmetric in the other, which results in a drastic lowering of the mesophase temperature range. The investigation of molecular arrangement is studied by x-ray diffraction (XRD) and the influence of the phase structure on molecular dynamics is analyzed on the basis of proton NMR relaxometry performed in a wide range of Larmor frequencies (20 kHz–100 MHz). The effect of the side-on linking of the mesogenic units becomes evident when the results are compared to those of the end-on bond dendrimers. In order to examine the impact of the linkage of the mesogenic arms to the dendritic core, the relaxation rate has been examined both for a tetrapode and for the corresponding monomer.

The organosiloxane tetrapodes, discussed in this paper, have been an object of previous studies by different techniques, namely, IR spectroscopy [17], deuterium NMR spectroscopy [18], dynamic light scattering [19], dielectric relaxation [20], and differential scanning calorimetry (DSC) [21]. Both of the compounds under study exhibit the nematic phase in a wide temperature range (~40 K in one case and ~80 K in the other) and show biaxial nematic ordering in part of the nematic range. This fact has been corroborated by different independent experimental techniques [17–19]. The detailed discussion on the phase structure and on molecular dynamics in this paper is intended to contribute also to the understanding of the factors leading to the biaxial nematic phase in organosiloxane tetrapodes.

II. EXPERIMENT

A. Experimental techniques

The XRD on aligned samples was performed on a MAR345 diffractometer equipped with a graphite monochromator for the Cu $K\alpha$ radiation ($\lambda = 1.54$ Å) and a two-dimensional (2D) image plate detector. The samples were heated and the data acquired in the presence of a magnetic field using a home-built capillary furnace. The data sets were analyzed using the "FIT2D" software package available from the ESFR, Grenoble, France.

The proton spin-lattice relaxation times T_1 were measured over a broad frequency range using a home-built fast field-cycling spectrometer from 20 kHz to 4 MHz and a conventional pulsed NMR spectrometer (BRUKER SXP 4-100) between 4 and 100 MHz. The polarization and detection fields of the field-cycling spectrometer are 0.215 T (corresponding to a Larmor frequency of 9.1 MHz) and the switching time is in the range of 2–3 ms [22]. The NMR samples were sealed under moderate vacuum ($<10^{-4}$ Torr) in glass tubes. The measurements were performed after cooling the sample in the presence of the external magnetic field from the isotropic phase to the desired temperature. In this way the samples were uniformly oriented in the nematic phase, but only partially oriented in the smectic-*C* phase as revealed from the proton NMR spectra. The time dependence of magnetization was found to be monoexponential indicating a uniform T_1 in the sample. The experimental error of T_1 measurements was estimated to be less than $\pm 10\%$.

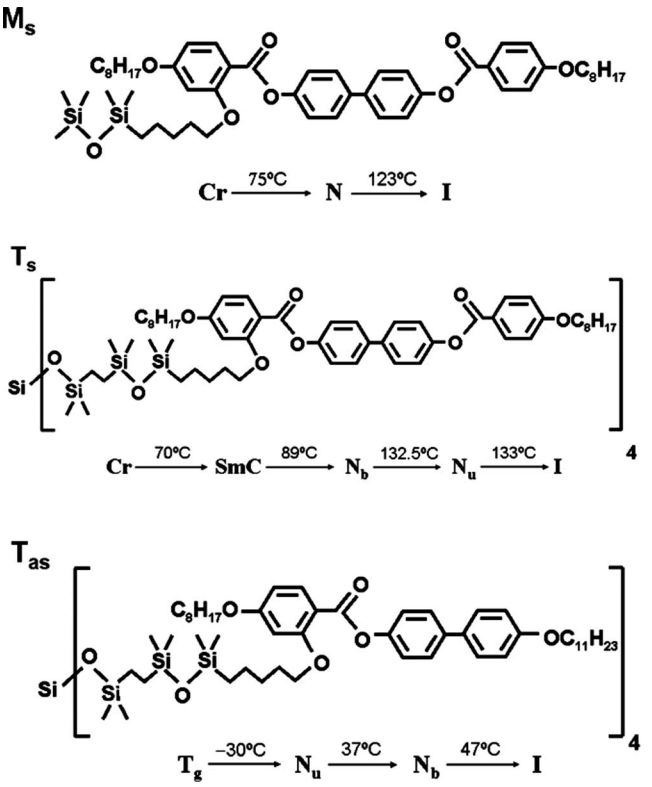

FIG. 1. Chemical formulas of the studied compounds and the corresponding phase sequences.

B. Description of the studied systems

Chemical structure of the studied compounds, their phase sequences, and the corresponding transition temperatures are presented in Fig. 1 [17]. Their synthesis is described in Ref. [23].

The monomeric liquid crystal, shortly referred to as M_s, with molecular mass 883.33 g mol^{-1} is a low-molecular-weight mesogenic compound composed of four aromatic rings connected by ester groups and two terminal octyloxy groups. It contains additionally a flexible chain of five methylene groups and a pentamethyldisiloxane group attached laterally to one of the aromatic rings. This compound exhibits the nematic phase between 75 °C and 123 °C.

The compound herein referred to as T_s (molecular mass 3910.06 g mol^{-1}) is an organosiloxane tetrapode based on four M_s molecules linked to the central core. The subscript *s* emphasizes the symmetric character of the mesogenic group. The flexible spacers which link the four mesogenic units to the central siloxane core are formed by five methylene groups and tetramethyldisiloxane group each. The material exhibits the phase sequence: Cr→70 °C→Sm*C*→89 °C →N_b→132.5 °C→N_u→133 °C→*I*. The nematic phases

(biaxial N_b and uniaxial N_u) appear at somewhat higher temperatures than in the monomeric M_s. The linking of M_s molecules into the tetrapode structure gives rise also to the formation of the smectic-*C* phase, which is absent in the monomeric constituent. The temperature transition between the biaxial and uniaxial nematic phases is reported in Ref. [17].

The third compound, shortly referred to as T_{as} (molecular mass 3597.96 g mol^{-1}), differs from T_s in the number of the aromatic groups and in the lengths of the aliphatic chains of the mesogenic unit. The mesogenic units contain here three aromatic rings (in contrast to four in T_s) and one longer alkyl chain formed by 11 methylene groups. The total length of the mesogen, however, is approximately the same in the extended configuration as in T_s. Though the overall structures of the tetrapodes T_s and T_{as} do not differ considerably, the T_{as} system exhibits the nematic phases at temperatures which are almost 100 K below the nematic range of T_s and has no smectic-*C* phase. The temperature transition between the biaxial and uniaxial nematic phases is reported in Ref. [17]. The biaxial nematic ordering has been confirmed by deuterium NMR spectroscopy observations in a mixture of this compound with a nematic deuterated probe [18]. The N_b-N_u temperature observed in that experiment is different must probably due to the presence of the probe [18]. The fact that the N_u-N_b phase transition is not observed in a recent DSC study means that a very small transition heat must be related to it [21]. This observation agrees with previous measurements of a similar phase transition for a bent core mesogen [24].

C. Detailed comparison between T_s and T_{as} molecular structures

For the forthcoming discussion of the molecular organization within the mesophases formed by tetrapodes, it will be useful to schematize their molecular structures by taking into account different chemical natures of specific molecular segments. It is worthwhile to note that generally the effect of microsegregation between molecular components with different properties (e.g., polar aromatic cores vs apolar aliphatic chains) is an important driving mechanism in the formation of liquid-crystalline phases. In the smectic phases the aromatic and aliphatic moieties are arranged in such a way that aromatic and aliphatic smectic sublayers alternate [25]. In the case of siloxane liquid-crystalline compounds, a third type of molecular segments, the siloxane chains, is involved, leading potentially to more complex microsegregated structures [26–28]. Evidence for this effect in organosiloxane tetrapodes has been presented in Ref. [16].

The calculated dimensions of molecular segments for the tetrapodes in the present study are shown in Fig. 2. The most extended configuration is considered as indicative of molecular dimensions for aliphatic and siloxane chains, which are otherwise flexible and adopt variable configurations in the liquid-crystalline state. In the figure, a planar representation is shown for simplicity, though it should be kept in mind that the central siloxane core has a tetrahedric (sp_3) bond geometry leading to a three-dimensional molecular structure. By

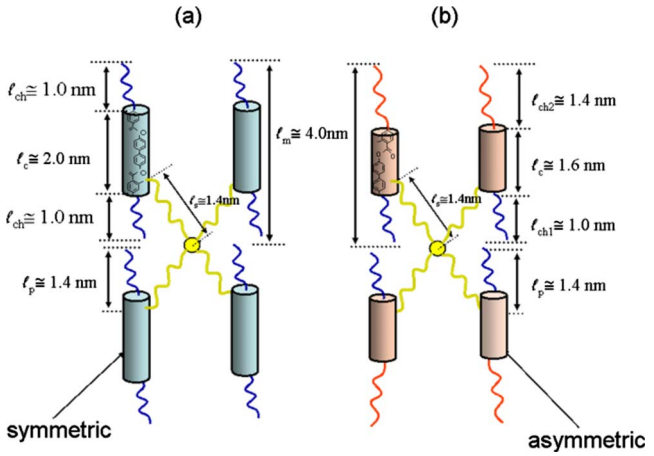

FIG. 2. (Color online) Molecular dimensions of tetrapodes T_s (a) and T_{as} (b) resulting from molecular modeling: ℓ_m—length of the mesogenic unit; ℓ_c—length of the aromatic core; ℓ_{ch}, ℓ_{ch1}, and ℓ_{ch2}—lengths of aliphatic chains; ℓ_s—length of the siloxane chains; ℓ_p—approximate distance from the aliphatic chains end to the oxygen atom at the chemical bond between aromatic core and siloxane chain.

comparing the structures of the tetrapodes T_s and T_{as}, it can be seen that the overall molecular dimensions are similar. The dendrimer core, constituted by the four siloxane chains linked to the central silicon atom, is identical for both molecules. The position of the side-on linker of each mesogenic unit to the respective siloxane chain is also the same in both tetrapodes. Moreover, it must be recalled that the dimensions of the mesogenic units, which include the aromatic core and the alkyl chains on both ends of it, are also similar in the two dendrimers. The difference in the self-organization of the two tetrapodes may thus be related to the symmetry properties of the respective mesogenic units. In the case of T_s, the chemical structure of the mesogenic unit is symmetric with respect to the plane perpendicular to the bond between the two central aromatic rings. It is possible to define two identical parts of the mesogenic unit, one of which is laterally connected to the dendrimer core. In the T_{as} compound such a symmetry does not exist. This difference might be crucial for the formation of mesophases and their structures in the two liquid-crystalline dendrimers under study.

III. RESULTS AND DISCUSSION: XRD STRUCTURAL CHARACTERIZATION

A. T_s tetrapode—smectic-*C* phase

The phase structures of the compounds discussed in this work were investigated by x-ray diffraction in samples aligned by the magnetic field. The resulting two-dimensional x-ray diffraction patterns, obtained as a function of temperature, were analyzed considering the angles defined in Fig. 3 (magnetic-field direction: vertical). θ is the scattering angle associated with the scattering vector magnitude $q = 4\pi \sin(\theta)/\lambda$. ψ and χ are the azimuthal angles corresponding to the small and wide scattering angle regions, respectively. The XRD pattern of the tetrapode T_s, recorded at

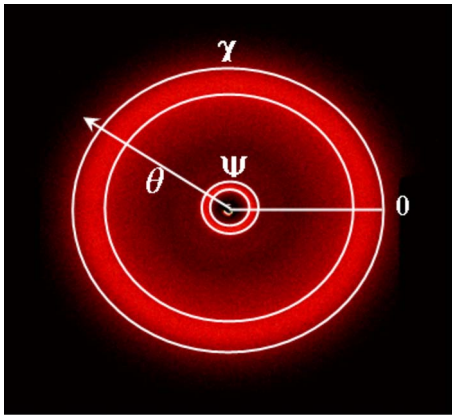

FIG. 3. (Color online) Schematic representation of the angular scales and integration limits used in the analysis of XRD diffraction patterns (magnetic-field direction: vertical). Plots as a function of θ (or the scattering vector magnitude $q=4\pi \sin \theta/\lambda$) are azimuthally integrated from 0 to 2π. Plots of azimuthal variation in the small- or wide-angle regions (variables ψ and χ, respectively) are radially integrated over θ with integration limits defined by circular crowns as exemplified in the picture.

78 °C, as a representative for the Sm*C* phase, is shown in Fig. 4(a). The corresponding azimuthally integrated XRD pattern (intensity versus scattering vector magnitude q) is presented in Fig. 4(b).

The pattern shown in Fig. 4(a) is characteristic of a smectic phase with two-dimensional liquidlike organization within the layers and indicates a tilt of molecules with respect to the layer's normal. The two sharp peaks in the small-angle region (in angle ψ as defined in Fig. 3), which are well fitted by Lorentzian curves, correspond to the first- and second-order pseudo-Bragg reflections associated with smectic layers of thickness $\ell \cong 3.1$ nm [Fig. 4(b)]. The evidence of a second-order diffraction peak reveals a high degree of smectic order within the sample. The angular dispersion of the pseudo-Bragg reflections in the small-angle region is due to a noncomplete orientation of the sample in the magnetic field. The asymmetric diffuse band observed at wide angles may be fitted by two Gaussian curves centered at q values associated with the distances ~0.44 nm and ~0.68 nm, respectively. The diffuse band at 0.44 nm corresponds to the lateral distance between aromatic segments and aliphatic chains within the smectic layers with liquidlike order. The band at 0.68 nm is typical of a liquidlike arrangement of the siloxane moietes [28].

Comparing the smectic layer thickness $\ell \cong 3.1$ nm with the molecular dimensions (see Fig. 2), it is natural to assume that the elements that define the smectic structure are the mesogenic units (of length $\ell_m \cong 4.0$ nm) and not the whole tetrapode. The fact that the smectic layers thickness is smaller than the mesogenic unit length is typical of a Sm*C* phase. Based on the conjecture that mainly the mesogenic units form the layered structure, it may be deduced that, if two of the mesogens belonging to a given tetrapode are included in a certain smectic layer, the other two mesogens of the same molecule belong to one of the adjacent layers. Considering steric and entropic reasons, this leads to a phase

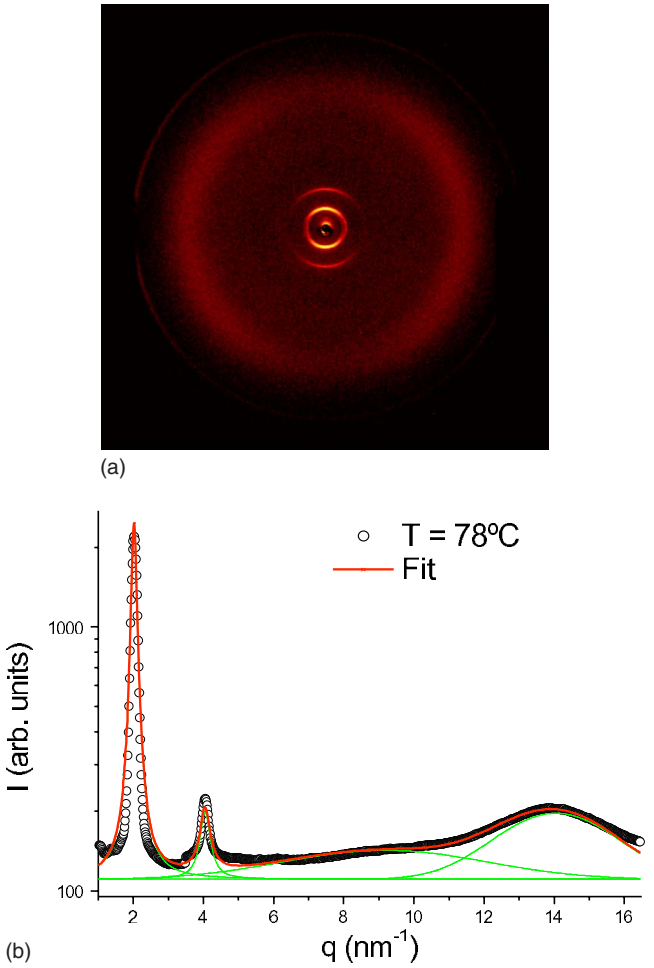

FIG. 4. (Color online) (a) Two-dimensional XRD pattern for T_s in the Sm*C* phase at 78 °C. (b) Fit of the azimuthally integrated XRD pattern (intensity vs scattering vector magnitude, $q=4\pi \sin \theta/\lambda$) for T_s in the Sm*C* phase at 78 °C.

structure as depicted in Fig. 5(a), where the smectic layers are formed by interdigitated mesogenic units belonging to different tetrapodes and with the central siloxane centers located approximately at the border between adjacent layers.

The proposed molecular organization for the Sm*C* phase ensures the microsegregation of the aromatic cores packed in between two sublayers formed by a mixture of aliphatic and siloxane chains. The fact that the mesogenic units are laterally attached to the dendrimer core inhibits the microsegregation between aliphatic and siloxane segments in a lamellar arrangement in contrast to the tetrapodes with terminally attached mesogens [16]. It should be noticed that in Fig. 5(a) the mesogenic units belonging to a given tetrapode are schematically represented in the plane of the page though the molecular structure of the tetrapode is actually not planar as the respective dendritic cores show tetrahedric symmetry.

The smaller value of the smectic layers' thickness in comparison with the mesogenic unit length clearly indicates the tilt of molecules typical for a Sm*C* phase. The tilt angle cannot be measured directly from the two-dimensional XRD pattern in view of a noncomplete alignment of the sample in the magnetic field. However, it is possible to get further in-

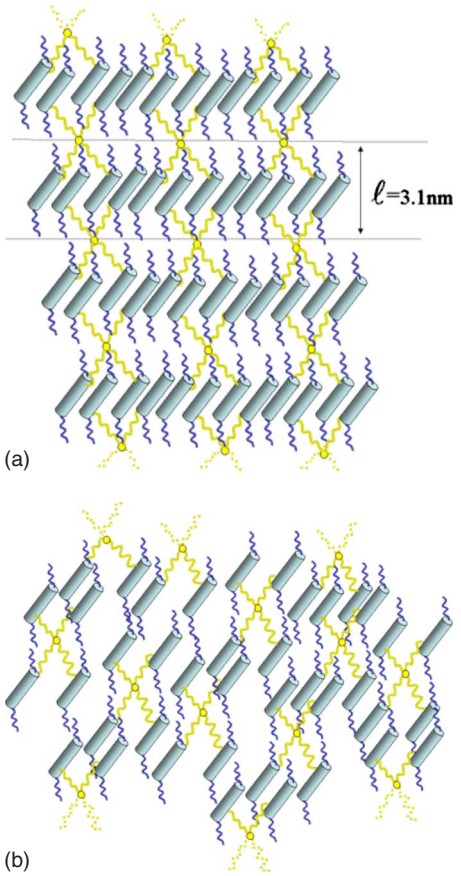

FIG. 5. (Color online) Proposed packing models for the SmC (a) and N phases (b) of the T_s tetrapod with side-on attached symmetric mesogenic units.

sight into the molecular organization considering the steric properties of different molecular segments (rigid elongated aromatic cores and flexible aliphatic and siloxane chains) microsegregated in smectic sublayers. This analysis can be done in terms of the molecular area Σ, which is defined as the area per molecule in the plane of a layer, given by $\Sigma = V/\ell$, where V is the molecular volume and ℓ is the smectic layer thickness.

The molecular volume for the tetrapode, estimated from the molecular mass and density (which is close to 1 g/cm^3 in this type of materials), is approximately 6.5 nm^3 at 78 °C, resulting in a molecular area of ~ 2.1 nm^2. The molecular area per monomer is $\Sigma_m = \Sigma/4 \sim 0.52$ nm^2. Considering the schematic representation of the local molecular organization within the SmC phase in Fig. 5(a), we can see that the cross section of two aromatic cores in the aromatic sublayer should match the sum of cross sections of two aliphatic chains and one siloxane chain in the aliphatic/siloxane sublayer. This leads on average to

$$\Sigma_m = \Sigma_c = \Sigma_{ch} + \frac{1}{2}\Sigma_s, \tag{1}$$

where Σ_c, Σ_{ch}, and Σ_s stand for the molecular areas of the aromatic core and aliphatic and siloxane chains, respectively. For each ith molecular segment (aromatic, aliphatic, and siloxane) the area Σ_i is related to the corresponding transverse cross-sectional area σ_i by the expression

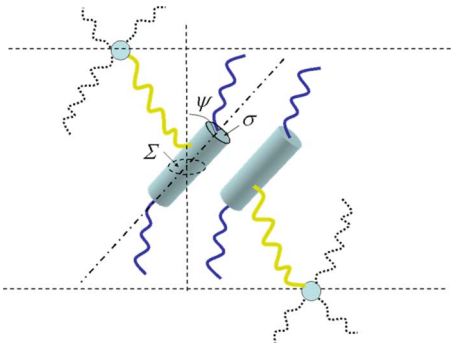

FIG. 6. (Color online) Schematic details of the SmC phase molecular organization with the indication of the molecular area (Σ), molecular cross-sectional area (σ), and tilt angle of the aromatic core (ψ).

$$\sigma_i = \Sigma_i \cos \psi_i, \tag{2}$$

where ψ_i is the tilt angle of the ith segment with respect to the normal to the smectic layer (see Fig. 6). Using expressions (1) and (2), we obtain the following relation between tilt angles and molecular cross-sectional areas:

$$\frac{\sigma_c}{\cos \psi_c} = \frac{\sigma_{ch}}{\cos \psi_{ch}} + \frac{1}{2}\frac{\sigma_s}{\cos \psi_s}. \tag{3}$$

The minimum value for the tilt angle of the aromatic core ψ_c corresponds to the case where $\cos \psi_{ch} = \cos \psi_s = 1$, assuming hypothetically that the disordered aliphatic and aromatic chains have no preferential tilting direction with respect to the normal to the layers. In this case Eq. (3) reads as

$$\frac{\sigma_c}{\cos \psi_c} = \sigma_{ch} + \frac{1}{2}\sigma_s = \Sigma_{ch} + \frac{1}{2}\Sigma_s = \Sigma_m. \tag{4}$$

Taking into account the estimated value for the molecular area of the monomer $\Sigma_m \sim 0.52$ nm^2 and the value of $\sigma_c \sim 0.24$–0.25 nm^2 typical for smectic liquid-crystalline phases [29], we obtain an approximate value of $\sim 61° - 62°$ for the tilt angle of the aromatic core with respect to the layer normal. The fact that the estimated value for Σ_m is compatible with sum $\sigma_{ch} + \frac{1}{2}\sigma_s$, if the typical values for the transverse cross-sectional areas of the siloxane chains (~ 0.43 nm^2) and of the aliphatic chains (~ 0.2–0.4 nm^2) [29] are inserted, corroborates the assumption that the tilt angles of the aliphatic and siloxane chains are negligible. Actually, the aromatic cores, having lower transverse cross-sectional area than the corresponding aliphatic/siloxane counterpart, are forced to tilt in order to compensate the difference in areas. This effect is responsible for the high value of the estimated tilt angle for this particular SmC phase. Such high values of tilt angle have been also found in the SmC phase of biforked mesogens, which possess two aliphatic chains at each end of the aromatic core [30].

The temperature dependence of the smectic layer thickness ℓ is plotted in Fig. 7. The layer thickness is close to 0.31 nm in the whole temperature range of the smectic-C phase

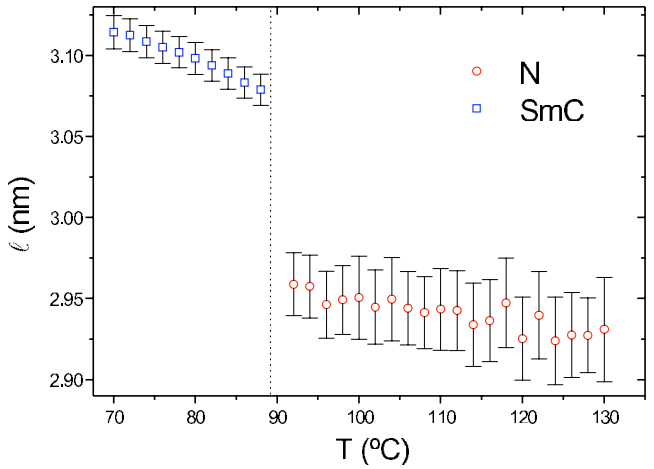

FIG. 7. (Color online) Variation in the layer spacing in the Sm*C* phase and the pseudolayer spacing (associated with the cybotactic groups) in the *N* phase as a function of temperature.

though a slight decrease with increasing temperature is observed. This decrease means that the tilt angle increases with increasing temperature, a fact in contrast with the usual behavior in liquid crystals with a Sm*C*-Sm*A* phase transition. If a Sm*C*-*N* transition occurs, the tilt angle is generally found to be temperature independent, which is here also not the case [31]. A slight increase in tilt angle with temperature has been observed in $\mathrm{Sm}C_{\mathrm{d}}$-$\mathrm{Sm}A_{\mathrm{d}}$ transitions of other organosiloxane compounds [16,28] and also in compounds exhibiting Sm*C*-isotropic transitions [32]. This unusual temperature dependence is readily understood in the present case if we take into account Eq. (4). When the temperature rises, the values of the cross-sectional areas of the disordered flexible chains, σ_{ch} and σ_s, increase. As the transverse cross-sectional area of the rigid aromatic core σ_c does not change significantly, this molecular segment is forced to increase the tilt ($\cos \psi_c$ decreases) in order to match the cross-sectional area of the corresponding aliphatic/siloxane sublayer.

B. T_s tetrapode—nematic phases

The XRD pattern for the nematic phases of the T_s compound, presented in Fig. 8(a), with four wide low-intensity off-meridional small-angle reflections, is typical of a nematic phase with a local Sm*C*-like order with a chevron-type arrangement. No difference in the XRD patterns was detected between the N_{b} and the N_{u} phase which is stable only over a very small temperature range. The azimuthally integrated patterns shown in Fig. 8(b) are well fitted by Gaussian curves corresponding to three diffuse bands associated with the distances 0.46, 0.65, and 2.95 nm. The bands at 0.46 nm and 0.65 nm correspond to the average lateral distance between aliphatic/aromatic molecular segments and between neighboring siloxane groups, respectively. The band at 2.95 nm is due to the pseudolayer spacing of the short-range Sm*C*-like order.

The existence of cybotactic groups, in which the smectic order is locally preserved in the nematic phase close to the nematic-smectic phase transition, is an often observed phenomenon in liquid crystals [33,34]. However, in the present case, this occurrence is observed in the nematic temperature domain as a whole showing that the Sm*C*-like molecular organization at local level [Fig. 5(b)] is a characteristic of the nematic phase in these materials and is clearly not only a pretransitional effect. The persistence of such XRD patterns in the nematic phase, far off from the nematic-isotropic transition, occurs in a number of compounds (monomers and octopodes) with similar mesogenic groups as those studied herein [35] and also in laterally functionalized oxadiazoles [36]. It is worthwhile to note that these small-angle reflections have also been discussed as an indication of biaxial nematic phase behavior [37].

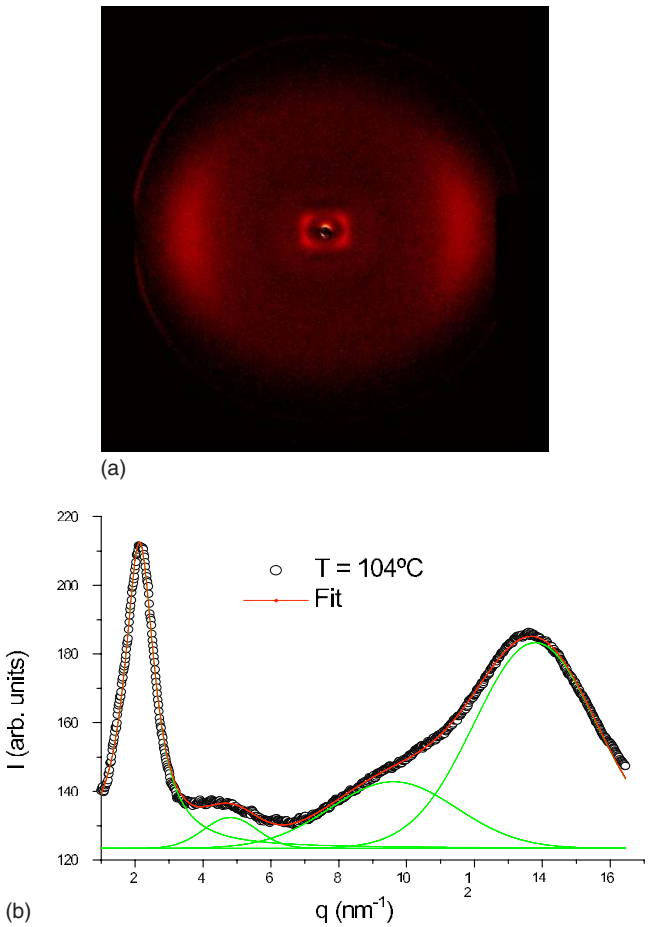

FIG. 8. (Color online) (a) Two-dimensional XRD pattern for T_s in the *N* phase at 104 °C. (b) Fit of the azimuthally integrated XRD pattern (intensity vs scattering vector magnitude, $q=4\pi \sin \theta/\lambda$) for T_s in the *N* phase at 104 °C.

The pseudolayer spacing within cybotactic groups is plotted as a function of temperature in Fig. 7. It has a nearly constant value of 2.95 ± 0.03 nm in a wide temperature range of about 40 K. At the *N*-Sm*C* transition there is a clear though small (~0.1 nm) discontinuity in ℓ. The tilt angle, which has not been directly accessible from the 2D XRD data for the Sm*C* phase (due to the noncomplete alignment of the sample in the magnetic field), is now easily measurable for the cybotactic clusters. It is obtained from the 2D XRD radially integrated pattern in the small-angle region [Fig. 9(a)]. The results for the tilt angle ψ_c (corresponding to

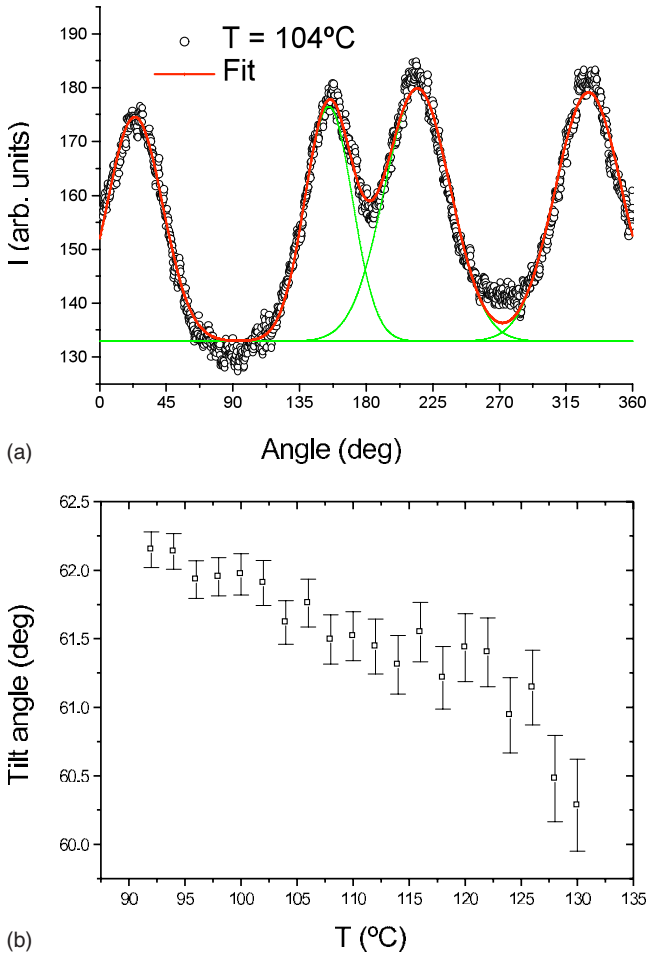

FIG. 9. (Color online) (a) Fit of the radially integrated XRD pattern in the small-angle region for T_s in the N phase at 104 °C. (b) Tilt angle of molecules with respect to the normal to the pseudolayers associated with the local SmC-like molecular organization in the N phase as a function of temperature.

the half-distance between the first and second peaks or between the third and fourth peaks) are presented in Fig. 9(b). The significant coincidence between these values and those determined from the molecular area estimate in the SmC phase clearly supports the packing model proposed for the SmC phase of these tetrapodes.

A schematic representation of the nematic phase is shown in Fig. 5(b). According to the model of molecular organization presented here, the transition from the SmC to the nematic phase occurs when the thermal agitation produces the breaking of the smectic layers into microdomains which preserve the orientational order and locally the positional order of the SmC-like structure. The breaking of the smectic layers allows for an easier orientation of mesogenic units along the magnetic field. Therefore, a uniform alignment of the sample could be achieved in the nematic phase in contrast to the smectic-C phase where the stability of the smectic layers prevails over the tendency to align with the field. The clustering is clearly a function of the chemical structure. Here it is worth to note that molecules with laterally connected mesogens exhibit mesophases at lower temperatures than those terminally connected with mesogenic units having a comparable number of aromatic groups. However, in lateral substituted systems the formation of nematic phase behavior is promoted. Local clustering of laterally connected mesogenes bearing microphase separating groups permits efficient packing of the molecules in the nematic phase [35] and has been discussed as well in detailed investigations of LC polymers [38,39]. It is also significant to stress that the clustering does not depend on the existence of a lower temperature SmC phase as will be put into evidence by the analysis of the XRD results on the compound T_{as}, which exhibits no smectic phase but a large temperature nematic domain where the cybotacticlike structures are evident over the whole nematic temperature range. Therefore, the existence of the a local smectic-C-like arrangement of the dendritic mesogenic cores must be understood as a property of the nematic phases of these particular materials, or in other words it is not a reminiscence of local packing from a more ordered phase.

Indeed the overall organization aligns well with the cluster model for the formation of the biaxial nematic phase [40,41]. Moreover, the similarity between the SmC phase and the N_b phase suggests that the possible symmetry of the N_b phase might not be confined to a D_{2h} symmetry but that an N_b phase with a C_{2h} symmetry can be formed. The difference to the SmC phase would be, as observed for this material, a loss of the long-range positional ordering.

C. T_{as} tetrapode—nematic phases

The T_{as} tetrapode, containing nonsymmetric mesogenic units, exhibits only nematic phases in a broad temperature range from −30 °C to 47 °C. The XRD recorded at 25 °C is presented in Fig. 10(a) and the corresponding azimuthally integrated XRD pattern, i.e., intensity versus scattering vector magnitude, $q=4\pi \sin(\theta)/\lambda$, is shown in Fig. 10(b).

The results for this compound are very similar to those obtained for the nematic phase of T_s. The x-ray diffraction pattern in the small-angle region shows that, also in the nematic phase of T_{as}, there are clusters with the smectic-C structure [this can be seen from x-ray data in Fig. 10(a)]. Such cybotactic assemblies are present throughout the nematic phase and are an inherent consequence of the dendritic molecular architecture. The azimuthally integrated XRD pattern in Fig. 10(b) exhibits an asymmetric broad band at wide angles which can be fitted by two Gaussian curves corresponding to the aliphatic/aromatic lateral average distance of 0.45 nm and to the average distance of 0.66 nm between siloxane groups. The values of the tilt angle of mesogenic units' cores in the SmC-like clusters are obtained from the fitting of the radially integrated XRD pattern in the small-angle region [Fig. 11(a)]. The evolution of the local tilt angle with temperature is presented in Fig. 11(b). The tilt angle ψ_c is slightly smaller in T_{as} than in the T_s tetrapode; it decreases from 56° at 25 °C to 51° close to the transition into the isotropic phase. No discontinuity can be observed at the N_b to N_u transitions. This observation is in line with the results of recent high-resolution colorimetric studies of this material [21] supporting a model where at the N_b to N_u transition clusters of suitably shaped molecules increase in size.

The chemical structure and dimensions of T_{as} tetrapode are quite similar to those of T_s tetrapode. This similarity and

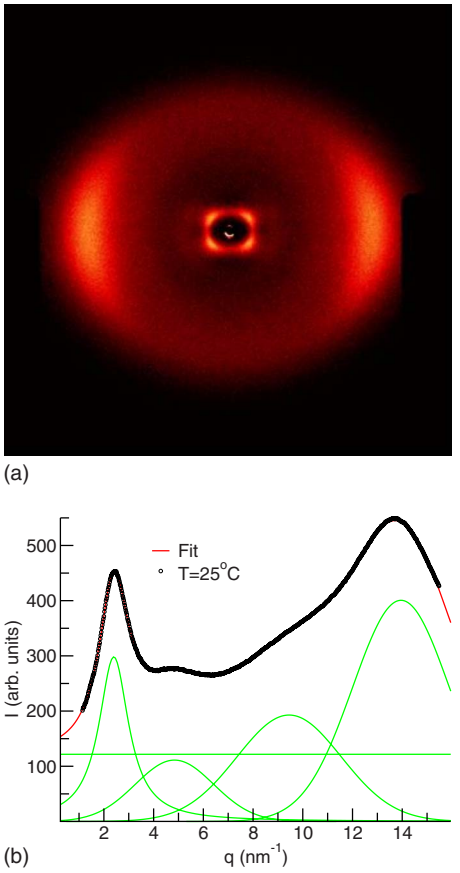

FIG. 10. (Color online) (a) Two-dimensional XRD pattern for T_{as} in the N phase at 25 °C. (b) Fit of the azimuthally integrated XRD pattern (intensity vs scattering vector magnitude, $q = 4\pi \sin \theta/\lambda$) for T_{as} in the N phase at 25 °C.

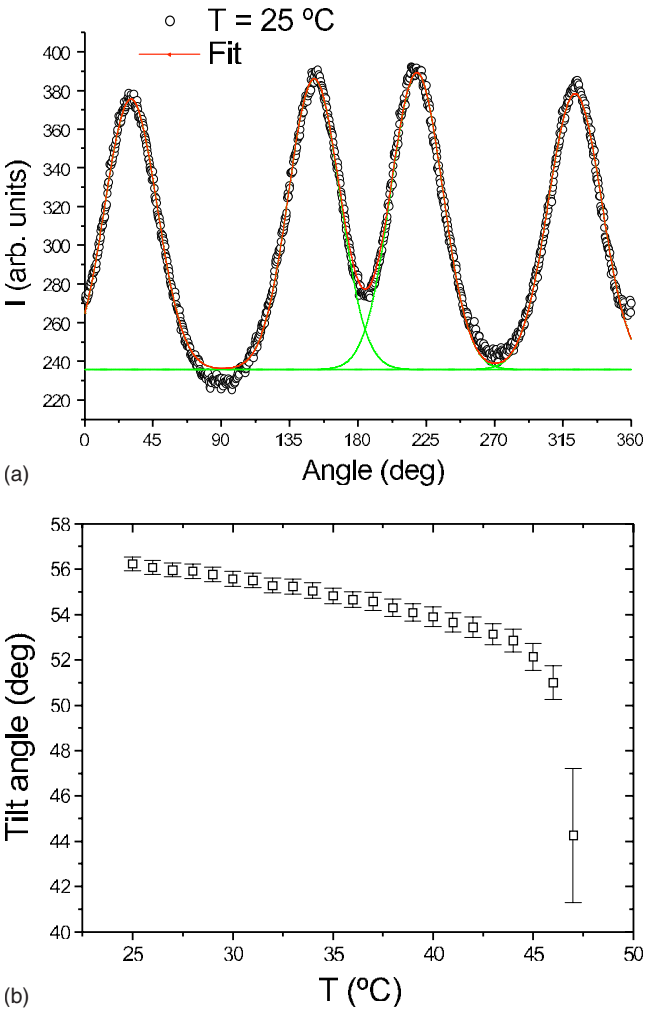

FIG. 11. (Color online) (a) Fit of the radially integrated XRD pattern in the small-angle region for T_{as} in the N phase at 25 °C. (b) Tilt angle of molecules with respect to the normal to the pseudolayers associated with the local SmC-like molecular organization in the N phase as a function of temperature.

the formation of the SmC-like cybotactic clusters suggest the possibility a formation of an N_b phase with a C_{2h} symmetry. However, in the molecular organization of the system there is an important difference with the T_s material discussed above. The asymmetry of T_{as} mesogenic units, with chains of different lengths in each side of the aromatic core, hinders the formation of aliphatic/siloxane sublayers of uniform thicknesses and the side-by-side packing of the aromatic cores. As shown in Fig. 12, two interdigitated mesogens belonging to T_{as} tetrapodes of adjacent hypothetical layers would not fit efficiently into an aligned microsegregated structure of aromatic and aliphatic/siloxane sublayers. This is in contrast to the T_s tetrapode where the symmetry of mesogenic units allows for an effective segregation. Such packing restrictions are most probably the reason that the T_{as} tetrapode—instead of forming the smectic-C phase—preserves the nematic structure to very low temperatures and favors the occurrence of biaxial nematic ordering with high values of the asymmetry parameter η as observed by deuterium NMR spectroscopy [18].

IV. RESULTS AND DISCUSSION: MOLECULAR DYNAMICS FROM NMR RELAXOMETRY DATA

A. Experimental results

Frequency dependences of the spin-lattice relaxation rates T_1^{-1} obtained for the monomeric system M_s and for the T_s and T_{as} tetrapodes are presented in Fig. 13. They were recorded at different temperatures to cover all mesophases of the studied compounds: isotropic, nematic, and SmC phase of the T_s tetrapode.

The spin-lattice relaxation rate of the *monomeric M_s system* exhibits the same type of frequency dispersion as ordinary liquid crystals. This includes a plateau below ~10 MHz and a decrease in T_1^{-1} above this frequency in the isotropic phase, and a frequency-dependent T_1^{-1} in the whole frequency range in the nematic phase [Fig. 13(a)]. However, the T_1^{-1} frequency dependence below ~10 MHz in the nematic phase of M_s is considerably weaker than in common calamitic liquid crystals such as PAA or 8CB [42–44].

The T_1^{-1} dispersions for the *tetrapode of symmetric mesogenic units T_s* are presented in Fig. 13(b). We see that the relaxation rate in T_s in the kilohertz frequency range is definitely faster than in M_s and that the slope of the dispersion curves is considerably steeper. Most importantly, frequency-dependent T_1^{-1} appears in T_s already in the isotropic phase at frequencies where a plateau is observed in the M_s system. It

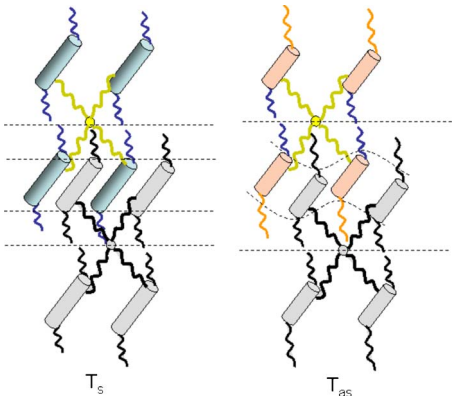

FIG. 12. (Color online) Comparison between local molecular packing for the T_s and T_{as} tetrapodes. The symmetry of T_s mesogenic units allows for an effective segregation between aromatic and aliphatic/siloxane sublayers. The asymmetric mesogenic units of T_{as}, with chains of different lengths in each side of the aromatic core, hinder the formation of aromatic and aliphatic sublayers of uniform thickness.

is also worth noting that there is no particular difference in the dispersions between the nematic and smectic-*C* phases in T_s which means that the onset of quasi-long-range positional order does not affect the relaxation process. Above 10 MHz, the decrease in T_1^{-1} with increasing temperature is similar for all phases.

In the *tetrapode of asymmetric mesogenic units* T_{as}, there is surprisingly no change in the T_1^{-1} frequency dispersion behavior on going from the isotropic into the nematic phase [Fig. 13(c)]. In both phases T_1^{-1} decreases monotonically with increasing frequency [45]. The slope of the dispersion curves is evidently larger than in the T_s tetrapode. The strong frequency dispersion in the isotropic phase, observed below 10 MHz both in T_s and T_{as} tetrapodes but absent in M_s, suggests the presence of slow molecular dynamics in tetrapodes. It is due to the attachment of monomer units to the central siloxane core, where they partly lose their rotational and translational motional freedom. Both dielectric and earlier NMR studies have revealed a slowing down of molecular dynamics in tetrapodes in comparison with the monomeric compounds [16,20].

B. Relaxation mechanisms and models

The analysis of proton spin-lattice relaxation data in terms of three relaxation mechanisms that account for the intermolecular and intramolecular modulations of proton dipolar interactions has been up to now successfully applied in a number of low-molecular-mass liquid crystals and in a tetrapode system [16,43,46–49]. The three main relaxation mechanisms are the following: (i) local molecular rotations/reorientations (R), (ii) molecular translational self-diffusion (SD), and (iii) collective orientational fluctuations (ODF). In view of the differences between the time scales of these dynamic processes, the total relaxation rate can be calculated as the sum of the three contributions,

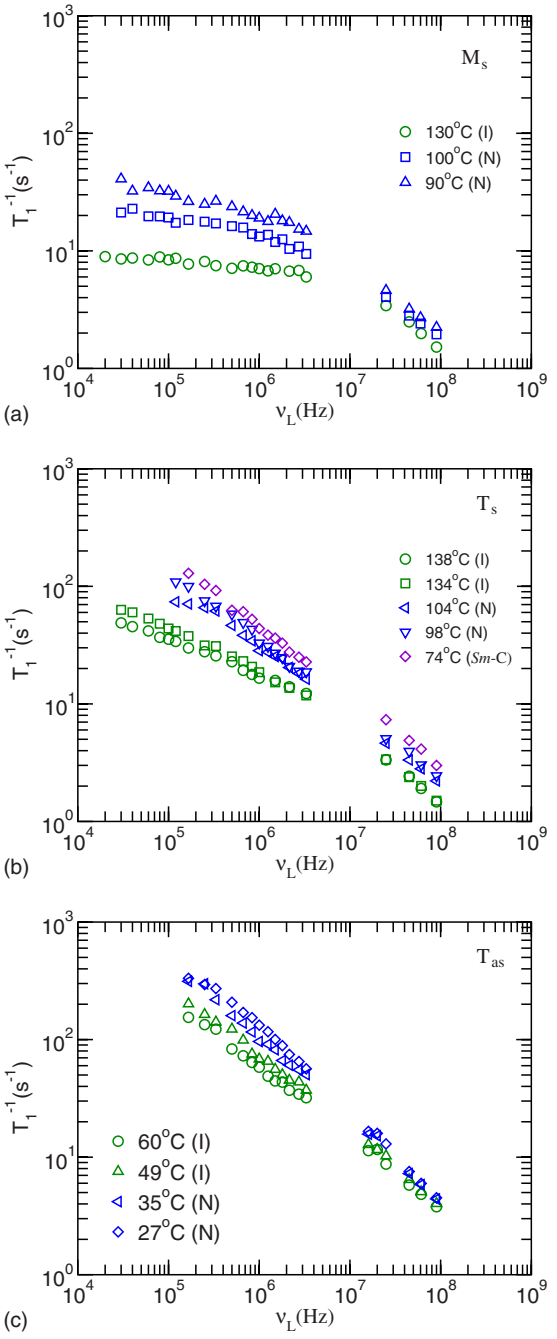

FIG. 13. (Color online) T_1^{-1} dispersion curves in the isotropic, nematic, and smectic-*C* phases of the studied compounds: (a) low-molecular-weight symmetric mesogen, M_s; (b) organosiloxane tetrapode with side-on attached symmetric mesogens, T_s; (c) organosiloxane tetrapode with side-on attached asymmetric mesogens, T_{as}.

$$\left(\frac{1}{T_1}\right) = \left(\frac{1}{T_1}\right)_R + \left(\frac{1}{T_1}\right)_{ODF} + \left(\frac{1}{T_1}\right)_{SD}. \quad (5)$$

Naturally, the above relaxation mechanisms are affected by the specific details of molecular organization in tetrapode systems.

(i) *Local molecular rotations/reorientations* (R) include rotational motion of the large tetrapode molecule as a whole, reorientations of mesogenic arms which are hindered by the

attachment to the central siloxane core though still relatively independent in view of long flexible spacers, and conformational changes in individual atomic groups. A T_1^{-1} dispersion, though measured in the range of four decades, does not contain enough information to detect details in the dynamics of the complex tetrapode molecule. Therefore, in the first approximation we describe the local rotational contribution to the relaxation rate, $(T_1^{-1})_R$, with only one correlation time. The correlation time, evaluated from the experimental data within such a simplified model, is usually characteristic of the slowest dynamic process among those which are effective for the relaxation within the NMR range. The relaxation rate caused by a stochastic process with the correlation time τ_R is described by the BPP (Bloembergen, Purcell, Pound) equation [42]

$$\left(\frac{1}{T_1}\right)_R(\nu_L,A_R,\tau_R)=A_R\left(\frac{\tau_R}{1+4\pi^2\nu_L^2\tau_R^2}+\frac{4\tau_R}{1+16\pi^2\nu_L^2\tau_R^2}\right), \tag{6}$$

where A_R is a constant depending on the strength of intramolecular interproton interactions and ν_L is the Larmor frequency.

(ii) *Molecular translational self-diffusion* (SD) in liquid crystals is an effective relaxation mechanism operating via the time modulation of intermolecular proton interactions. In the tetrapode mesophases, it is reasonable to assume that translational self-diffusion of molecules is strongly restricted due to the interdigitation of tetrapode arms. The effect of translational displacements of a molecule as a whole is therefore most probably negligible, its time scale being out of the NMR relaxometry detection range. However, faster noncorrelated displacements of mesogenic arms provide a similar kind of time modulation of interactions among protons on neighboring arms, even if they occur within the same molecule. In the lack of a theory developed for such a case, we describe the contribution of translational displacements, $(T_1^{-1})_{SD}$, by the Torrey's analytical model originally developed for isotropic liquids [50].

Within this model the relaxation rate depends on the spins' density n, distance of closest approach between spins in neighboring arms d, and the mean displacement time τ_D.

(iii) *Collective orientational fluctuations* in the nematic phase, usually called order director fluctuations (ODF), yield a contribution to the relaxation rate of the following form:

$$\left(\frac{1}{T_1}\right)_{ODF}(A_{ODF},\nu_L,\nu_{c\,\max},\nu_{c\,\min})=A_{ODF}\frac{1}{\nu_L^{1/2}}\left[g\left(\frac{\nu_{c\,\max}}{\nu_L}\right)-g\left(\frac{\nu_{c\,\min}}{\nu_L}\right)\right],$$

$$g(a)=\frac{1}{\pi}\left[\arctan(\sqrt{2a}+1)+\arctan(\sqrt{2a}-1)-\operatorname{arctanh}\left(\frac{\sqrt{2a}}{a+1}\right)\right]. \tag{7}$$

Here A_{ODF} is a constant which depends on the viscoelastic properties of the material and on the strength of intramolecular proton interactions; $\nu_{c\,\max}$ and $\nu_{c\,\min}$ are the high and low cutoff frequencies of director modes with wave number q defined as $Kq_{\max}^2/(2\pi\eta)$ and $Kq_{\min}^2/(2\pi\eta)$, respectively [42]. K denotes an average elastic constant and η is the effective viscosity. In the M_s system, the laterally attached flexible chain may disturb the nematic order but it is reasonable to assume that the three-dimensional character of order director fluctuations is not affected. In the tetrapodes, the interdigitation of mesogenic units of neighboring molecules favors the establishment of high orientational order.

It should be mentioned that the $\nu_L^{-1/2}$ frequency dependence [Eq. (7)] is a consequence of the quadratic dependence of the decay time of ODF modes on their wavelength and of the three-dimensional character of the nematic phase. In the smectic phases, which are quasi-two-dimensional in view of their layered structure, those ODF modes that represent layer undulations give rise to the ν_L^{-1} frequency dependence of T_1^{-1}. In a previous paper we studied the proton relaxation of an end-on liquid-crystalline tetrapode and found three local rotational modes associated with the motion of tetrapode arms as well as collective undulations of the mesogenic interlayers [16]. As a matter of fact, the specific structure of the dendrimer mesophase allowed the first observation of the relaxation induced by layer undulations in the whole kilohertz range.

It should be also mentioned that the dendrimers T_s and T_{as} exhibit biaxial ordering in part of the nematic temperature range [17–19]. However, the biaxiality is not expected to be relevant for the proton NMR relaxometry results. Namely, a large number of proton pairs involved in the dipolar interactions responsible for the spin-lattice relaxation rate (in particular in less ordered flexible chains) are not affected by the biaxiality. Moreover, the significantly large values of the biaxiality parameter in these compounds are observed at temperatures out of the range of the present NMR work [18]. Similar restrictions, related to the observation of the effect of biaxial ordering on molecular dynamics, were reported in the dielectric relaxation studies of the same compounds [20].

C. Analysis and discussion of T_1^{-1} dispersions

The experimental proton spin-lattice relaxation results were analyzed using a global nonlinear least-squares minimization procedure in which Eqs. (5)–(7) were fitted simultaneously to experimental T_1^{-1} data at different temperatures considering the expected relaxation mechanisms in each mesophase.

1. M_s compound

The T_1^{-1} dispersion in the isotropic phase of the monomeric system—not close to the phase transition—can be well described by a superposition of R and SD contributions to the relaxation rate. In the nematic phase, the ODF contribution is included. The free parameters in the fits are τ_R, τ_D, d, A_{ODF}, and $\nu_{c\,\max}$ [Eq. (7)]. As for the strength of rotational contribution, we used the fixed value $A_R=1.5\times10^9$ s^{-2} estimated from the previous study of a siloxane system [16]. The density of spins $n\cong5.05\times10^{28}$ m^{-3} was calculated from the mass density ~1 g/cm^3 typical of liquid-crystalline com-

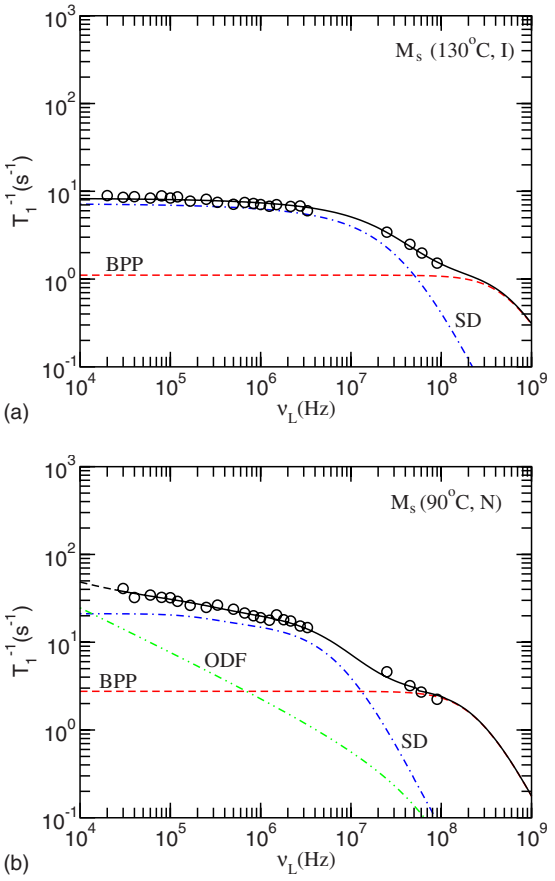

FIG. 14. (Color online) Frequency dispersions of the proton spin-lattice rate T_1^{-1} for the M_s system in the (a) isotropic phase (130 °C) and (b) nematic phase (90 °C). The solid lines were obtained by fitting Eqs. (5)–(7) to the experimental data and represent the sum of contributions of ODF, SD, and molecular reorientations of the BPP type.

pounds. The cutoff frequency $\nu_{c\,\min}$ could not be determined from the fits with a reasonable accuracy as it falls out of the accessible range of Larmor frequencies.

The T_1^{-1} experimental data and the theoretical curves corresponding to the best global fits are presented in Figs. 14(a) and 14(b) for the isotropic phase at $T=130$ °C (7 K above the *N-I* transition) and for the nematic phase at 90 °C. The best-fitted values of adjustable parameters are presented in Table I. The results show that the dispersion curve in the isotropic phase is quite similar in magnitude and shape to that of low-molecular-mass calamitic liquid crystals, e.g., 8CB [42]. This means that the M_s lateral chain with the siloxane end group does not basically affect the nature of the relaxation process in the isotropic phase. Still, the diffusion displacement time in the isotropic M_s is somewhat longer than in 8CB which results in the prevailing role of SD as the relaxation mechanism below ~50 MHz. Local reorientations become the leading relaxation mechanism only at frequencies above this value. A SD contribution stronger than usually observed in nematic phases appears also in the nematic phase of M_s. The ODF contribution, on the other hand, is relatively weak. In fact, the ODF strength is about ten times smaller than in conventional calamitic compounds. This effect might be associated with the disturbed orientational order due to the presence of the siloxane chain laterally attached to the mesogenic core. The correlation times τ_R, obtained from the fits both in the isotropic and nematic phases (see Table I), show an Arrhenius-type temperature dependence, $\tau_R=\tau_\infty \exp(E_a/kT)$, with the activation energy $E_a \sim 30$ kJ/mol.

2. T_s system

In Fig. 15 we present, as examples, the best fits of the theoretical model to the experimental data in the isotropic ($T=138$ °C), nematic ($T=112$ °C), and smectic-*C* ($T=78$ °C) phases of the T_s tetrapode. The values of the best-fitting parameters τ_R, τ_D, d, A_{ODF}, and $\nu_{c\,\max}$ are presented in Table I. All fits were performed using a fixed strength $A_R=1.5\times10^9$ s^{-2} and spin density $n\sim5\times10^{28}$ m^{-3}, i.e., the same values as for the M_s system. These values are physically reasonable since the chemical structure of the T_s dendritic arms, including the mesogenic units, is identical to the monomer M_s.

In the isotropic phase, the T_1^{-1} dispersion clearly shows an unexpected increasing in the relaxation rate with decreasing frequency below 200 kHz [Fig. 15(a)]. Such a run of the dispersion curve is not present in the monomeric system and implies the presence of another relaxation mechanism in addition to *R* and SD. According to the fit, the additional relaxation mechanism has a $\nu_L^{-1/2}$ frequency dependence which will be discussed later. The correlation times for translational displacements in T_s are slightly larger than in the M_s monomer and so is the distance of closest approach between neighboring spins d. This is certainly associated with the

TABLE I. Model parameters obtained from the fits of Eqs. (5)–(7) to the experimental data in the three liquid-crystalline systems.

	M_s			T_{as}				T_s					
	I	*N*		*I*		*N*		*I*		*N*		Sm*C*	
T (°C)	130	100	90	60	49	35	27	138	134	112	98	78	74
τ_R (10^{-10} s)	1.5	3.0	3.8	5.1	7.3	7.6	8.2	1.7	1.9	2.4	3.1	3.9	4.3
A_{ODF} (10^4 s$^{-3/2}$)		0.13	0.24	6.3	8.2	12	15	0.68	1.0	3.2	3.8	4.6	4.9
$\nu_{c\,\max}$ (10^7 Hz)		~10	~10	5.3	3.2	3.0	2.5	8.0	5.0	5.0	5.0	5.0	5.0
τ_D (10^{-9} s)	2.9	9.1	15					7.3	7.6				
d (10^{-10} m)	5.0	5.0	5.0					5.5	6.0				

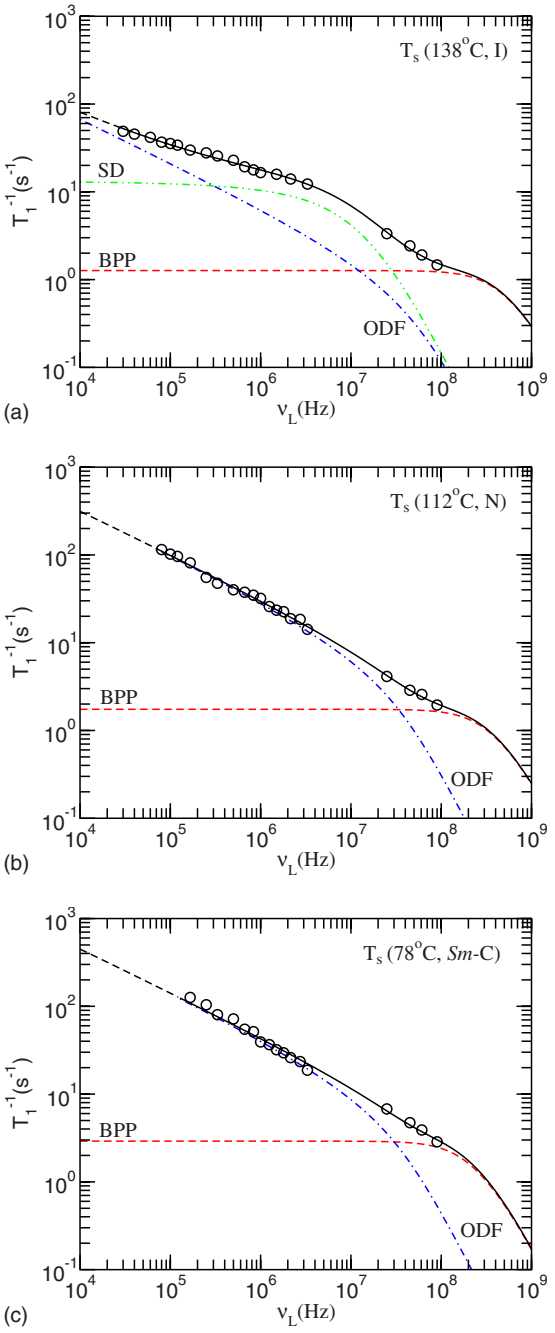

FIG. 15. (Color online) Frequency dispersions of the proton spin-lattice rate T_1^{-1} for the T_s tetrapode in the (a) isotropic phase (138 °C), (b) nematic phase (112 °C), and (c) Sm*C* phase (78 °C). The solid lines were obtained by fitting Eqs. (5)–(7) to the experimental data and represent the sum of contributions of ODF, SD, and BPP-type reorientations of mesogenic units.

restrictions imposed by the linkage of the mesogenic units to the central siloxane core. The SD contribution in the isotropic phase might arise either from the motion of tetrapode molecules as a whole or just from the restricted and noncorrelated translational displacements of individual mesogenic units.

In the nematic and smectic-*C* phases, the T_1^{-1} dispersion behavior [Figs. 15(b) and 15(c)] is well explained by the contributions of order director fluctuations and rotations/reorientations mechanisms without taking into account the self-diffusion. Its inclusion into the relaxation model would not improve the fit. The negligible role of the SD mechanism is most probably due to the interdigitation of tetrapode molecules extended to relatively large domains and preventing, in the limit, molecular translational displacements to occur.

When discussing the T_1^{-1} dispersions in the isotropic and in the two mesophases of the T_s tetrapode, we observe that a contribution proportional to $\nu_L^{-1/2}$ is essential to explain the relaxation rate in all three phases. As described in the previous section, this type of contribution is characteristic of collective orientational fluctuations, i.e., fluctuations of director in the nematic phase. The same frequency dependence has been found also in the smectic-*C* phase of some calamitic compounds due to the in-plane fluctuations of the tilting direction [46]. In the isotropic phase, the $\nu_L^{-1/2}$ dispersion appears often as a pretransitional effect of local nematic order and is detected close to the isotropic-nematic transition [42,51]. It is caused by the presence of cybotactic assemblies which possess short-range orientational and sometimes also positional order. Notably, in the T_s case, the $\nu_L^{-1/2}$ dispersion is evident much farther above the *N-I* phase transition than in common liquid crystals. Moreover, it is totally absent in the monomeric analog M_s. The reason for the easy formation of cybotactic clusters in the isotropic phase of T_s is the specific tetrapode molecular structure that favors the interdigitation of mesogenic arms belonging to adjacent tetrapodes and facilitates in this way the local formation of order.

The fitted $\nu_L^{-1/2}$ dispersion curve in the isotropic phase of T_s exhibits a high frequency cutoff but no leveling off at low frequencies in the range where the measurements have been performed. The absence of the low-frequency cutoff above 10^5 Hz allows for an estimate of the smallest possible size $\xi_{\min}$ of ordered clusters compatible with the experimental data. Taking into account an effective viscosity ~ 10 times larger with respect to the monomer sample ($\eta \sim 0.6$ N s m^{-2}), elastic constant $K \sim 10^{-11}$ N, and the expression $\xi \cong [\pi K/(2\eta\nu_{c\,\min})]^{1/2}$, one obtains $\xi_{\min} \sim 15$ nm. The estimate shows that the cybotactic clusters are larger than ~ 15 nm a few K above the transition into the nematic phase. The existence of cybotactic clusters in the isotropic phase of T_s is supported also by the wide-angle XRD results (Fig. 16). The radial integrated x-ray pattern has an angular dependence with maxima at 0° and 180° that confirms the local alignment of mesogenic units.

The strength of the ODF relaxation mechanism A_{ODF} in T_s increases continuously with decreasing temperature from about $A_{ODF}=0.68\times10^4$ s$^{-3/2}$ at 138 °C in the isotropic phase to $A_{ODF}=4.9\times10^4$ s$^{-3/2}$ at 74 °C in the Sm*C* phase. These values are higher than those obtained for the nematic phase in the M_s system and might be partly due to the expected increase in the viscosity in T_s. A slight decrease observed in the high cutoff frequency of the ODF relaxation mechanism could be ascribed to the same reason. Another factor, increasing the strength of director fluctuations in T_s, is a higher degree of orientational order.

The T_1^{-1} dispersion in the smectic-*C* phase of T_s deserves a bit of special attention. It follows strictly the $\nu_L^{-1/2}$ law without a contribution of modes associated with layer undulations that would be recognized through a ν_L^{-1} frequency

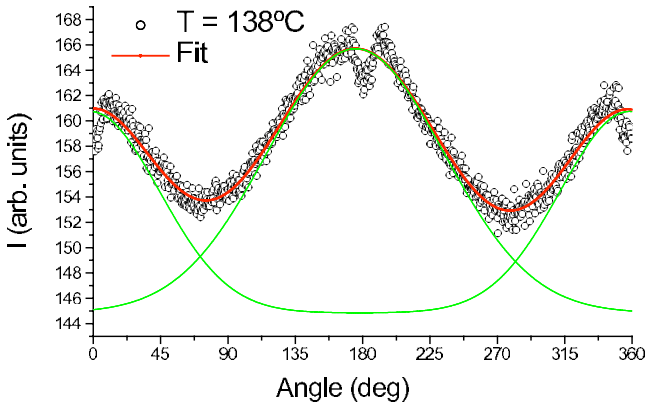

FIG. 16. (Color online) Fit of the radially integrated x-ray pattern in the wide-angle region in the isotropic phase of the T_s tetrapode 5 °C above the *N-I* transition. It reveals the presence of cybotactic clusters.

dependence. Obviously, the contribution of layer undulations is totally overwhelmed by the in-plane director fluctuations in the present case, which is surprising in view of an exactly opposite situation in the smectic-*C* phase of end-on dendrimers [16]. The lack of observed layer undulations in the smectic-*C* phase of the side-on tetrapode might be due to the compact structure of sublayers with interpenetrating alkyl/siloxane chains. Such a structure would not allow for an independent motion of aromatic layers and has therefore a damping effect on the long-wavelength undulations.

In what concerns the rotations/reorientations relaxation mechanism, the corresponding correlation times vary from $\tau_R = 1.7 \times 10^{-10}$ s at 138 °C to $\tau_R = 4.3 \times 10^{-10}$ s at 74 °C following an Arrhenius temperature dependence with an activation energy of about 15 kJ/mol and a prefactor $\tau_\infty \sim 2.5 \times 10^{-12}$ s. A smaller activation energy than in M_s suggests that only partial molecular segments are involved in the detected rotations and not the whole molecule.

3. T_{as} system

The experimental relaxation data and the fitted curves calculated according to Eqs. (5)–(7) are presented in Figs. 17(a) and 17(b) for the isotropic (T=60 °C) and nematic phase (T=27 °C) of the T_{as} tetrapode, respectively. Equally good fits were obtained for dispersions obtained at other temperatures in all phases of T_{as}. The best-fit values of three adjustable parameters are presented in Table I. The fits were performed considering R and ODF as the relevant relaxation mechanisms, both in the isotropic and in the nematic phase. An inspection of the experimental data namely shows that the T_1^{-1} dispersions are relatively smooth and might be reasonably well explained by two relaxation mechanisms only. In principle, a small contribution of SD cannot be ruled out, but its inclusion does not improve the fits. A similarly negligible role of self-diffusion has been found in the mesophases of T_s (previous section) and ascribed to the restrictions of translational mobility due to the interdigitation of mesogenic units of neighboring tetrapode molecules.

An interesting point is that the ruling out of self-diffusion appears in T_{as} already in the isotropic phase, whereas it was

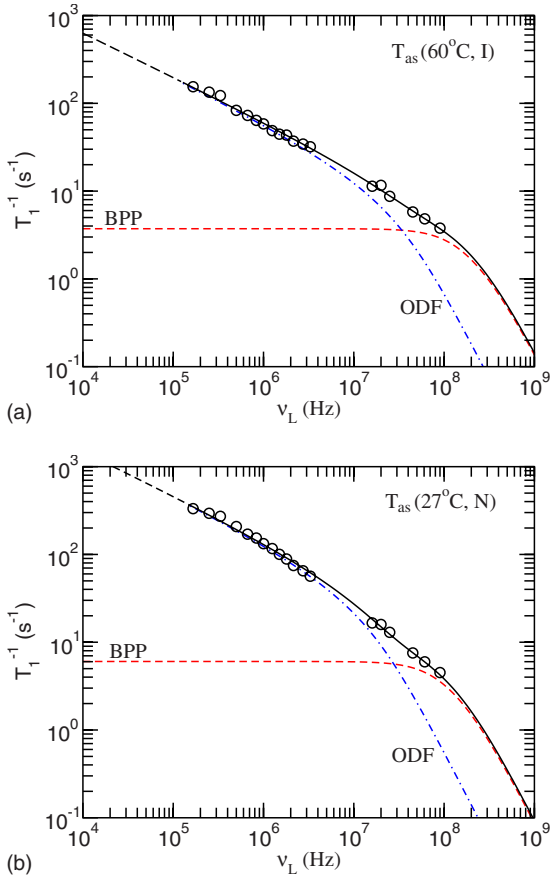

FIG. 17. (Color online) Frequency dispersions of the proton spin-lattice rate T_1^{-1} for the T_{as} tetrapode in the (a) isotropic phase (60 °C) and (b) nematic phase (27 °C). The solid lines are the fit of Eqs. (5)–(7) to the experimental data and represent the sum of contributions of ODF and reorientations of mesogenic units of the BPP type. The contribution of self-diffusion is negligible.

limited to the mesophases in T_s. This dissimilarity might be connected with a huge difference in the temperature range of the corresponding isotropic phases (there is more then 80 K difference between the *N-I* transition temperatures of both compounds). Due to the much lower *N-I* transition in T_{as}, it is reasonable to assume that—apart from the increased viscosity—the interdigitation of neighboring molecules is extended to larger domains already in the isotropic phase what reduces the translational diffusive motion. The conjecture of larger domains of interdigitated molecules and enhanced viscosity is supported by the relative magnitude of the $\nu_L^{-1/2}$ contribution which is clearly larger in T_{as} than in the case of T_s. The corresponding strength A_{ODF} in T_{as} exceeds its counterpart by almost ten times (Table I). On the other hand, the high cutoff frequency in T_{as} is found smaller than in T_s—another argument in favor of increased viscosity.

Similar characteristic features related to the ODF relaxation mechanism appear also in the nematic phase. A_{ODF}, which is related to the viscoelastic properties of the material, rises in T_{as} up to 1.5×10^5 $s^{-3/2}$, which is a large value in comparison with T_s and with majority of other nematic liquid crystals. Correspondingly, the high cutoff frequency is relatively small. Both effects can be explained by the increased value of the viscosity at low temperatures.

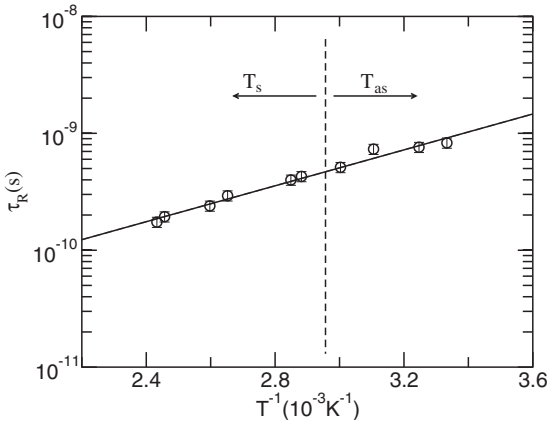

FIG. 18. Plot of the fitted rotations/reorientations correlation time τ_R for the T_s and T_{as} tetrapodes as a function of the inverse temperature. The solid line represents the fit of the Arrhenius expression to the experimental values. The activation energy and τ_∞ are the same for both tetrapodes: 15 kJ/mol and $\sim 2.5\times 10^{-12}$ s, respectively.

The rotations/reorientations contribution to the relaxation rate in T_{as} has been calculated with the fixed geometric factor $A_R=1.5\times 10^9$ s^{-2}, the same as in M_s and T_s systems. This assumption is reasonable in view of the similarity between the mesogenic unit of T_{as} and those of T_s and M_s. In the three cases, the lengths of the mesogenic units (rigid body +terminal alkyl chains) are practically equal (considering their extended configuration) and the rigid bodies are essentially of the same type. The values of the fitting parameter τ_R in T_{as} vary from $\tau_R=5.1\times 10^{-10}$ s at 60 °C to $\tau_R=8.2\times 10^{-10}$ s at 27 °C. They exhibit the Arrhenius temperature behavior with an activation energy identical to that of the T_s tetrapode (see Fig. 18). Moreover, the prefactor τ_∞ turns out to be the same for both compounds. The rotational motion detected by NMR is obviously independent of the symmetric/asymmetric nature of the mesogenic arm.

V. CONCLUSIONS

In this paper we present a study of two organosiloxane tetrapode compounds with laterally attached mesogenic units (T_s and T_{as}). The monomeric compound (M_s), consisting precisely of mesogenic units and linking chains of the T_s tetrapode, was added for comparison. The joint analysis of x-ray diffraction data and proton NMR relaxation frequency dispersion curves provides a way to seek for the understanding of the relation between the complex phases' structure and the molecular dynamics in such materials. The specific properties of dendrimers investigated in this work derive from the effect of connecting four chemically identical branches to a single central core. By comparing the results obtained for the monomer M_s and for the corresponding dendrimer T_s, it becomes evident how the covalent central bonding of the mesogenic units influences both the phase structure and molecular dynamics in such systems. It is remarkable how the central linkage induces orientational/positional order by favoring the interdigitation of mesogenic units belonging to neighboring molecules. This feature becomes clearly evident when comparing the liquid-crystalline phases in the T_s tetrapode with those of the corresponding monomer M_s. The T_s's polymorphism includes uniaxial nematic, biaxial nematic, and Sm*C* phases [17], while the laterally substituted monomers alone, with exactly the same chemical structure as the dendrimer arms, give rise to a single nematic mesophase. The packing models proposed within this work, both for the nematic and particularly for the Sm*C* phase of T_s, illustrate how interdigitation of the mesogenic units, induced by their linkage to the central siloxane core, favors the decreasing of rotational and translational degrees of freedom with the appearance of local order. In fact, the analysis of the x-ray diffraction results on both the Sm*C* and *N* phases of the tetrapode puts into evidence the effect of microsegregation between the aromatic cores on one side and the aliphatic and siloxane chains on the other. It should be noted that in tetrapodes with side-on attached mesogenic arms the nonaromatic sublayers consist of a mixture of aliphatic and siloxane chains, whereas the microsegregation in end-on tetrapodes included separate sublayers of each of these types of chemical segments. The microsegregation effect and the relative dimensions of the molecular segments in T_s and T_{as} give rise to a "Sm*C*-like" local packing with a large tilt angle ($\sim 60°$) even in the *N* (and N_b) phases. These cybotactic clusters do not appear only as a pretransitional effect but persist through the whole temperature range of the *N* phase. This suggests the formation of the N_b phase with a C_{2h} symmetry. The comparison between the structural properties of the two dendrimers T_s and T_{as}, on the other hand, leads to the conclusion that the symmetric structure of T_s mesogenic units allows for the layered packing (Sm*C* phase) due to an effective microsegregation between the aromatic and the aliphatic/siloxane molecular segments. In the case of T_{as}, the relative dimensions of the molecular segments of the monomers prevent the aromatic cores of mesogenic units, belonging to interdigitated adjacent molecules, from "fitting" efficiently in a planar sublayer as discussed in detail before. The Sm*C*-like packing is thus limited to cybotactic clusters in the nematic phase.

The local ordering effect, arising from the special molecular structure of the tetrapodes, is clearly reflected on molecular dynamics as shown by the analysis of NMR proton relaxometry results. The branched molecular structure of the tetrapodes imposes rotational and translational restrictions to the motion of mesogenic units. Moreover, the interdigitation of tetrapode arms also limits the motion of each tetrapode molecule as a whole. As discussed before, a few subtle effects have been observed by comparing molecular dynamics of the two tetrapodes, T_s and T_{as}, but their main relaxation behavior is essentially similar.

The experimental T_1^{-1} frequency dependences of the three compounds under study are explained in terms of three relaxation mechanisms: director fluctuations, translational self-diffusion, and local reorientations. Their relative importance in the monomeric compound M_s does not differ considerably from conventional calamitic liquid crystals in spite of the alkyl/siloxane chain, laterally added to the mesogenic part. Its disordering effect is recognized in a somewhat diminished strength of director fluctuations. The situation is different in

tetrapodes, where the linking of monomeric units to the central siloxane core has a significant impact on the spin relaxation process, resulting from the structural changes in different phases.

Nematiclike director fluctuations, which produce a T_1^{-1} contribution proportional to $\nu_L^{-1/2}$, turn out to play the leading role in all phases of tetrapodes. Their presence in the isotropic phase is an indicator of cybotactic clusters far above the *N-I* transition. Obviously, the interdigitation of mesogenic units in adjacent tetrapode molecules facilitates the formation of clusters with short-range orientational and possibly also positional order. In this way, the remaining local orientational ordering in the isotropic phase, associated with the clusters, allows for the existence of nematiclike order fluctuations justifying the unusual T_1^{-1} contribution proportional to $\nu_L^{-1/2}$ in the isotropic phase instead of the typical flat frequency dispersion [45]. The $\nu_L^{-1/2}$ contribution in the asymmetric tetrapode is larger than in the symmetric one, most probably due to the occurrence of the *N-I* transition at a much lower temperature. In the nematic phase, the long-range order allows for strong director fluctuations with modes extending over a wide dynamic range. The same type of the dispersion curve persists in T_s upon cooling into the smectic-*C* phase. Therefore, the T_1^{-1} dispersion is not able to discern the local clusters with the smectic-*C* structure in the nematic phase. They were, however, unambiguously detected by the x-ray diffraction. In the smectic-*C* phase a difference emerges between the director fluctuations observed in tetrapodes with end-on mesogenic units [16] and those with side-on mesogenic groups, which are discussed in the present work. In the former case, two-dimensional director fluctuations, i.e., out-of-plane undulations of smectic layers, were clearly visible via their characteristic $\sim\nu_L^{-1}$ contribution to T_1^{-1}. Actually, this represented the first case where layer undulations have been detected in a thermotropic liquid crystal by NMR in the whole kilohertz range. In the side-on tetrapode, on the other hand, it turns out that the director fluctuations enter only in the form of three-dimensional in-plane azimuthal fluctuations with $\nu_L^{-1/2}$ dispersion. Layer undulations are obviously damped by a more compact structure of the layers.

The role of translational self-diffusion in relaxing the proton spins is considerably diminished in tetrapodes. The fitting of theoretical expressions to experimental data requires a contribution of self-diffusion only in the isotropic phase of T_s. Its effect is prevailed by other relaxation mechanisms in all other phases. The translational mobility is reduced not only by the size and branched shape of tetrapode molecules; the largest impact comes probably from steric restrictions which lead to the interdigitation of mesogenic units. Even in the isotropic phase of T_s, the magnitude of the fitted displacement time suggests that it is related to the noncorrelated motion of dendrimer arms and not to the diffusion of molecules as a whole. The marginal effect of diffusion on the spin relaxation corroborates the proposed model for the phase structure of side-on tetrapodes.

The role of local rotations/reorientations in the relaxation process is rather small but evident in all phases. The corresponding correlation time is relatively short and is associated with a low activation energy. Obviously, NMR is detecting only one branch of rotational modes which is related to the reorientation of a smaller group of atoms. Other modes are either out of the NMR frequency range or hidden by stronger relaxation mechanisms. Dielectric measurements would be a more sensitive method for their study.

ACKNOWLEDGMENTS

This work was partially supported by the Portuguese Science and Technology Foundation (FCT) Contracts No. POCTI/34453/CTM/2000, No. ISFL/261/2008, and No. PTDC/FIS/65037/2006 (OE/Feder/FSE), and by the EU through Contracts No. HPRN-CT-2000-0016 and No. FP7-PEOPLE-2007-1-1-ITN-215884. The authors are also grateful for the financial support by the Slovenian Research and Development Agency (Grant No. P1-0099) and by the Portuguese FCT/GRICES through the bilateral Project No. BI-PT/08-09-003. M.C. thanks Calouste Gulbenkian Foundation and Instituto Superior Técnico, TU Lisbon for António da Silveira grant.

[1] V. Percec, W. D. Cho, and G. Ungar, J. Am. Chem. Soc. **122**, 10273 (2000); X. Zeng, G. Ungar, L. Yongsong, V. Percec, A. E. Dulcey, and J. K. Hobbs, Nature (London) **428**, 157 (2004); J.-M. Rueff, J. Barbera, B. Donnio, D. Guillon, M. Marcus, and J. L. Serrano, Macromolecules **36**, 8368 (2003); R. M. Richardson, E. V. Agina, N. I. Boiko, V. P. Shibaev, and I. Grillo, J. Phys. Chem. B **112**, 16346 (2008).

[2] G. R. Newkome, C. N. Moorefield, and F. Vögtle, *Dendrimers and Dendrons: Concepts, Syntheses, Applications* (Wiley-VCH, Weinheim, 2001).

[3] L. J. Mathias and T. W. Carothers, J. Am. Chem. Soc. **113**, 4043 (1991).

[4] D. A. Tomalia and H. D. Durst, in *Topics in Current Chemistry*, edited by E. Weber (Springer-Verlag, Berlin, 1993), Vol. 165, pp. 193–313.

[5] S. Uppuluri, S. E. Keinath, D. A. Tomalia, and P. R. Dvornic, Macromolecules **31**, 4498 (1998).

[6] S. Uppuluri, D. A. Tomalia, and P. R. Dvornic, in *Polymeric Materials Encyclopedia*, edited by J. C. Salamone (CRC Press, New York, 1996), Vol. 3, pp. 1824–1830.

[7] R. F. Service, Science **295**, 2398 (2002).

[8] M. Liu and J. M. J. Fréchet, Pharm. Sci. Technol. Today **2**, 393 (1999).

[9] E. C. Wiener, M. W. Brechbiel, H. Brothers, R. L. Magin, O. A. Gansow, D. A. Tomalia, and P. C. Lauterbur, Magn. Reson. Med. **31**, 1 (1994).

[10] M. F. Ottaviani, F. Furini, A. Casini, N. J. Turro, S. Jockusch, D. A. Tomalia, and L. Messori, Macromolecules **33**, 7842 (2000).

[11] R. M. Kim, M. Manna, S. M. Hutchins, P. R. Griffin, N. A.

Yates, A. M. Bernick, and K. T. Chapman, Proc. Natl. Acad. Sci. U.S.A. **93**, 10012 (1996).
[12] I. M. Saez and J. W. Goodby, Liq. Cryst. **26**, 1101 (1999).
[13] A. Van-Quynh, D. Filip, C. Cruz, P. J. Sebastião, A. C. Ribeiro, J.-M. Rueff, M. Marcos, and J. L. Serrano, Eur. Phys. J. E **18**, 149 (2005).
[14] A. Van-Quynh, D. Filip, C. Cruz, P. J. Sebastião, A. C. Ribeiro, J.-M. Rueff, M. Marcos, and J. L. Serrano, Mol. Cryst. Liq. Cryst. **450**, 191 (2006).
[15] V. Domenici, M. Cifelli, C. A. Veracini, N. I. Boiko, E. V. Agina, and V. P. Shibaev, J. Phys. Chem. B **112**, 14718 (2008).
[16] D. Filip, C. Cruz, P. J. Sebastião, A. C. Ribeiro, M. Vilfan, T. Meyer, P. H. J. Kouwer, and G. H. Mehl, Phys. Rev. E **75**, 011704 (2007).
[17] K. Merkel, A. Kocot, J. K. Vij, R. Korlacki, G. H. Mehl, and T. Meyer, Phys. Rev. Lett. **93**, 237801 (2004).
[18] J. L. Figueirinhas, C. Cruz, D. Filip, G. Feio, A. C. Ribeiro, Y. Frère, T. Meyer, and G. H. Mehl, Phys. Rev. Lett. **94**, 107802 (2005); C. Cruz, J. L. Figueirinhas, D. Filip, G. Feio, A. C. Ribeiro, Y. Frère, T. Meyer, and G. H. Mehl, Phys. Rev. E **78**, 051702 (2008).
[19] K. Neupane, S. W. Kang, S. Sharma, D. Carney, T. Meyer, G. H. Mehl, D. W. Allender, Satyendra Kumar, and S. Sprunt, Phys. Rev. Lett. **97**, 207802 (2006).
[20] K. Merkel, A. Kocot, J. K. Vij, G. H. Mehl, and T. Meyer, Phys. Rev. E **73**, 051702 (2006).
[21] G. Cordoyiannis, D. Apreutesei, G. H. Mehl, C. Glorieux, and J. Thoen, Phys. Rev. E **78**, 011708 (2008).
[22] D. M. Sousa, P. A. L. Fernandes, G. D. Marques, A. C. Ribeiro, and P. J. Sebastião, Solid State Nucl. Magn. Reson. **25**, 160 (2004); D. M. Sousa, G. D. Marques, P. J. Sebastião, and A. C. Ribeiro, Rev. Sci. Instrum. **74**, 4521 (2003).
[23] S. Diez, D. Dunmur, M. R. De La Fuente, P. Karahaliou, G. H. Mehl, T. Meyer, M. A. Perèz Jubindo, and D. J. Photinos, Liq. Cryst. **30**, 1021 (2003); R. Elsäßer, G. H. Mehl, J. W. Goodby, and D. J. Photinos, Chem. Commun. (Cambridge) **2000**, 851; T. Meyer and G. H. Mehl, 19th International Liquid Crystal Conference (unpublished).
[24] V. Prasad, S. W. Kang, K. A. Suresh, L. Joshi, Q. Wang, and S. Kumar, J. Am. Chem. Soc. **127**, 17224 (2005).
[25] A. Skoulios and D. Guillon, Mol. Cryst. Liq. Cryst. **165**, 317 (1988).
[26] M. Ibn-Elhaj, A. Skoulios, D. Guillon, J. Newton, P. Hodge, and H. J. Coles, Liq. Cryst. **19**, 373 (1995); J. Phys. II **6**, 271 (1996).
[27] E. Corsellis, D. Guillon, P. Kloess, and H. Coles, Liq. Cryst. **23**, 235 (1997).
[28] T. Múrias, A. C. Ribeiro, D. Guillon, D. Shoosmith, and H. J. Coles, Liq. Cryst. **29**, 627 (2002).
[29] M. Ibn-Elhaj, H. J. Coles, D. Guillon, and A. Skoulios, J. Phys. II **3**, 1807 (1993).
[30] A. C. Ribeiro, C. Cruz, H. T. Nguyen, S. Diele, B. Heinrch, and D. Guillon, Liq. Cryst. **29**, 635 (2002).
[31] S. Chandrasekhar, *Liquid Crystals*, 2nd ed. (Cambridge University Press, Cambridge, 1992).
[32] J. J. Benattar, F. Moussa, and M. Lambert, J. Chim. Phys. Phys.-Chim. Biol. **80**, 99 (1983).
[33] A. DeVries, Mol. Cryst. Liq. Cryst. **10**, 219 (1970).
[34] L. V. Azaroff, Proc. Natl. Acad. Sci. U.S.A. **77**, 1252 (1980).
[35] P. K. Karahaliou, P. H. J. Kouwer, T. Meyer, G. H. Mehl, and D. J. Photinos, Soft Matter **3**, 857 (2007); J. Phys. Chem. B **112**, 6550 (2008).
[36] D. Apreutesei and G. H. Mehl, J. Mater. Chem. **17**, 4711 (2007).
[37] B. R. Acharya, A. Primak, T. Dingmans, E. T. Samulski, and S. Kumar, Pramana, J. Phys. **61**, 231 (2003); B. R. Acharya, A. Primak, and S. Kumar, Phys. Rev. Lett. **92**, 145506 (2004); L. A. Madsen, T. J. Dingemans, M. Nakata, and E. T. Samulski, *ibid.* **92**, 145505 (2004).
[38] F. Hardouin, S. Mery, M. F. Archard, M. Mauzac, P. Davidson, and P. Keller, Liq. Cryst. **8**, 565 (1990).
[39] C. Pugh, P. Zhu, G. Kim, J. X. Zheng, M. J. Rubal, and S. Z. D. Cheng, J. Polym. Sci., Part A: Polym. Chem. **44**, 4076 (2006).
[40] A. G. Vanakaras and D. J. Photinos, J. Chem. Phys. **128**, 154512 (2008).
[41] R. Berardi, L. Muccioli, S. Orlandi, M. Ricci, and C. Zannoni, J. Phys.: Condens. Matter **20**, 463101 (2008).
[42] R. Y. Dong, *Nuclear Magnetic Resonance of Liquid Crystals*, 2nd ed. (Springer, Berlin, 1997) and references therein.
[43] M. Vilfan, T. Apih, P. J. Sebastião, G. Lahajnar, and S. Zumer, Phys. Rev. E **76**, 051708 (2007).
[44] W. Wolfel, F. Noack, and M. Stohrer, Z. Naturforsch. C **30a**, 437 (1975); J. Struppe and F. Noack, Liq. Cryst. **20**, 595 (1996).
[45] D. Filip, C. Cruz, P. J. Sebastião, A. C. Ribeiro, T. Meyer, and G. H. Mehl, Mol. Cryst. Liq. Cryst. **436**, 17 (2005).
[46] A. Carvalho, P. J. Sebastião, A. C. Ribeiro, H. T. Nguyen, and M. Vilfan, J. Chem. Phys. **115**, 10484 (2001).
[47] A. C. Ribeiro, P. J. Sebastião, and C. Cruz, Pramana, J. Phys. **61**, 205 (2003).
[48] A. C. Ribeiro, P. J. Sebastião, and C. Cruz, Mol. Cryst. Liq. Cryst. **362**, 289 (2001).
[49] V. Domenici, T. Apih, and C. A. Veracini, Thin Solid Films **517**, 1402 (2008).
[50] H. C. Torrey, Phys. Rev. **92**, 962 (1953); F. Harmon and B. H. Muller, *ibid.* **182**, 400 (1969).
[51] P. J. Sebastião, D. Sousa, A. C. Ribeiro, M. Vilfan, G. Lahajnar, J. Seliger, and S. Žumer, Phys. Rev. E **72**, 061702 (2005).